Human Molecular Genetics, 2020, Vol. 29, No. 12 1996–2003

doi: 10.1093/hmg/ddaa035
Advance Access Publication Date: 11 March 2020
General Article

GENERAL ARTICLE

Knockin mouse model of the human *CFL2* p.A35T mutation results in a unique splicing defect and severe myopathy phenotype

Samantha M. Rosen[1,2,3], Mugdha Joshi[1], Talia Hitt[1], Alan H. Beggs[2,3] and Pankaj B. Agrawal[1,2,3,*]

[1]Division of Newborn Medicine, Boston Children's Hospital, Harvard Medical School, Boston, MA 02115, USA, [2]Division of Genetics and Genomics, Boston Children's Hospital, Harvard Medical School, Boston, MA 02115, USA and [3]The Manton Center for Orphan Disease Research, Boston Children's Hospital, Harvard Medical School, Boston, MA 02115, USA

*To whom correspondence should be addressed at: Divisions of Neonatology & Genetics, Children's Hospital Boston, 300 Longwood Ave CLSB 15030, Boston, MA 02115, USA. Tel: +1 6179192153; Fax: +1 6177300253; Email: pagrawal@enders tch.harvard.edu

Abstract

Cofilin-2 is an actin-binding protein that is predominantly expressed in skeletal and cardiac muscles and belongs to the AC group of proteins, which includes cofilin-1 and destrin. In humans, cofilin-2 (*CFL2*) mutations have been associated with congenital myopathies that include nemaline and myofibrillar myopathy. To understand the pathogenicity of the human *CFL2* mutation, p.A35T, that first linked cofilin-2 with the human disease, we created a knock-in mouse model. The $Cfl2^{A35T/A35T}$ (KI) mice were indistinguishable from their wild-type littermates at birth, but they rapidly worsened and died by postnatal day 9. The phenotypic, histopathologic and molecular findings mimicked the constitutive *Cfl2*-knockout (KO) mice described previously, including sarcomeric disruption and actin accumulations in skeletal muscles and negligible amounts of cofilin-2 protein. In addition, KI mice demonstrated a marked reduction in *Cfl2* mRNA levels in various tissues including skeletal muscles. Further investigation revealed evidence of alternative splicing with the presence of two alternate transcripts of smaller size. These alternate transcripts were expressed at very low levels in the wild-type mice and were significantly upregulated in the mutant mice, indicating that pre-translational splicing defects may be a critical component of the disease mechanism associated with the mutation. Evidence of reduced expression of the full-length *CFL2* transcript was also observed in the muscle biopsy sample of the patient with p.A35T mutation.

Introduction

Nemaline myopathy (NM; also called rod myopathy or nemaline rod myopathy) is the most common histopathological form of congenital myopathy (CM), characterized by accumulation of sarcomeric proteins into fine, rod-like structures known as 'nemaline bodies' that are observably present in muscle biopsies (1–4). Although the NM phenotype is heterogeneous in terms of onset and severity, major clinical features of this disease include muscle weakness and hypotonia, which can lead to difficulties with breathing, feeding, speaking and motor control and can sometimes be fatal. The genetic basis of NM is highly heterogeneous with many genes linked to this

Received: September 10, 2019. **Revised:** February 26, 2020. **Accepted:** February 28, 2020

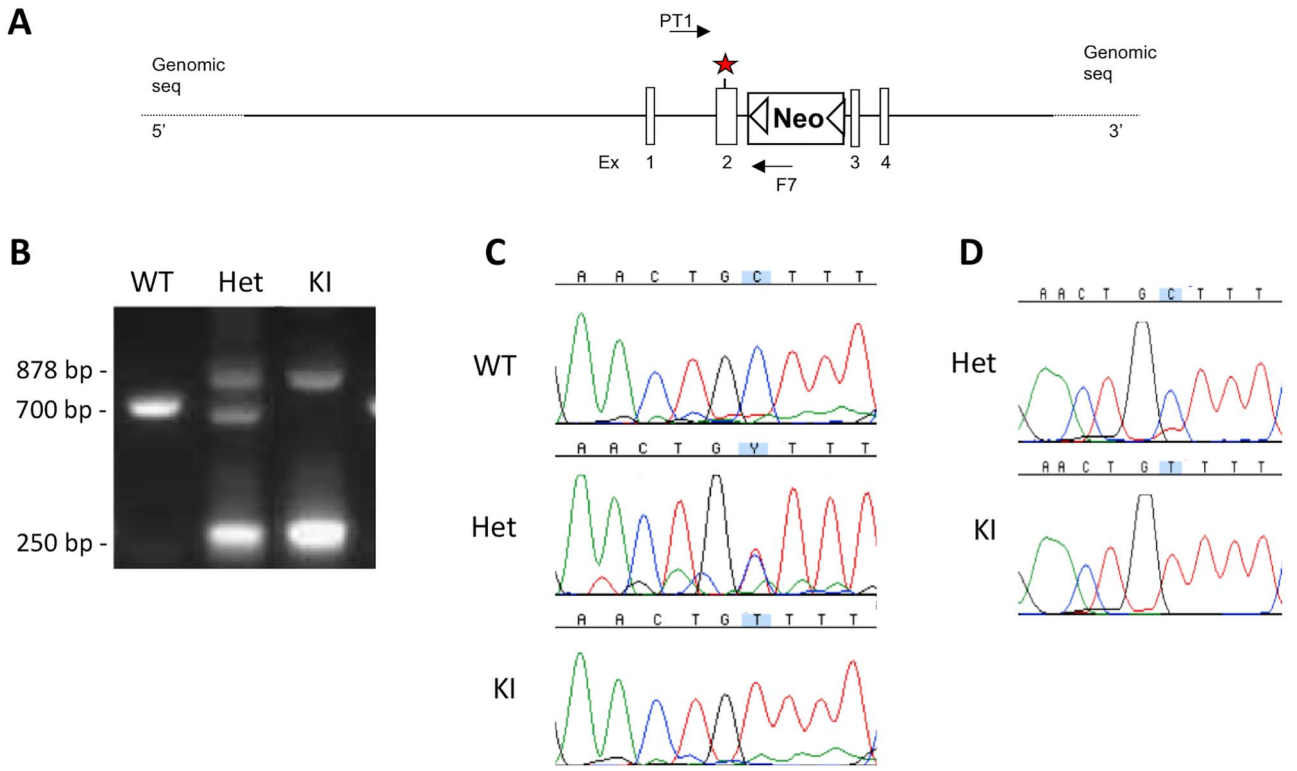

Figure 1. Gene targeting strategy to generate *Cfl2*$^{A35T/A35T}$ mice. **(A)** Targeting construct to create the p.A35T KI allele. The red asterisk above exon 2 indicates the location of the p.A35T mutation. The white arrowheads flanking the Neo cassette represent FRT sites, which were targeted by FLP for recombination. The locations of the genotyping primers (forward: PT1, Reverse, F7) are labelled with black arrows above and below the schematic. **(B)** PCR analysis of DNA isolated from WT, Het and KI mice. WT mice are represented by a single band at 700 bp and KI mice by a single band at 878 bp and Het mice are identifiable by the presence of both the WT and KI bands. An additional band at 250 bp is present only in Het and KI mice as a result of a primer that probes for a sequence located in the Neo cassette. **(C)** Sequencing chromatogram of the PCR product from DNA samples of WT, Het and KI mice shows the presence of the variant in homozygous and heterozygous states in KI and Het mice, respectively. **(D)** Sequencing chromatogram of the RT-PCR product derived from the RNA sample extracted from quadriceps muscle of Het and KI mouse confirming the variant.

condition including those encoding for sarcomeric thin filaments (5). We have previously identified *CFL2* as the sixth gene to cause NM in a single highly consanguineous family including two affected siblings (6). The proband's muscle showed nemaline bodies, minicores, concentric laminated bodies and areas of F-actin accumulation, while the affected sibling's muscle exhibited non-specific myopathic features. Both the proband and the affected sibling were homozygous for the missense mutation *CFL2* NM_021914.7:c.103G>A, predicted to result in an alanine-to-threonine substitution at residue 35 (p.A35T) (6). Since our initial identification of the gene, six additional cases of myopathy with novel mutations in *CFL2* have been reported, that link *CFL2* to both NM and myofibrillar myopathy (7–10). Furthermore, we have previously demonstrated that *Cfl2*-KO mice recapitulate the human myopathy with histopathological findings of myofiber degeneration, core-like lesions, extensive sarcomeric disruptions, nemaline bodies and F-actin accumulations (11). Other *Cfl2*-KO mouse models have also demonstrated actin-associated myopathic phenotypes (12).

To further understand the pathogenicity of human p.A35T *CFL2* mutation, we generated a *Cfl2*$^{A35T/A35T}$ knock-in mouse line carrying the same mutation (6). Here we report the phenotypic characterization of this mouse line, establishing its validity as a model of the human condition, and demonstrate a primary mechanism of pathogenesis common to the mouse and human mutations.

Results

Gene targeting and generation of *Cfl2*$^{A35T/A35T}$ mice

The murine cofilin-2 locus (*Cfl2*) was targeted by homologous recombination using a vector subcloned from a B6 BAC clone. A pGK-gb2 loxP/FLP recombinase target (FRT)-flanked Neo cassette was inserted downstream of exon 2, and the G>A point mutation in exon 2 was generated by PCR mutagenesis (Fig. 1A). The targeting vector was electroporated into C57BL/6 embryonic stem (ES) cells, and clones that underwent proper homologous recombination were confirmed by PCR and Southern blotting. Targeted ES cells were microinjected into Balb/c blastocysts. Resulting chimeras with a high percentage black coat color were mated C57BL/6 flippase recombinase (FLP)-homozygous mice, which were wild-type (WT) at the *Cfl2* locus, to remove the Neo cassette and generate F1 heterozygous offspring, which were then interbred to generate mice homozygous for the missense mutation. This occurred due to recognition and recombination of the FRT sequences flanking the Neo cassette by FLP, analogous to the Cre-*lox* system. Homozygous KI mice were screened by agarose gel analysis (Fig. 1B) and Sanger sequencing of PCR products (Fig. 1C). The presence of the mutation was confirmed in RNA extracted from various tissues including quadriceps muscle by Sanger sequencing (Fig. 1D).

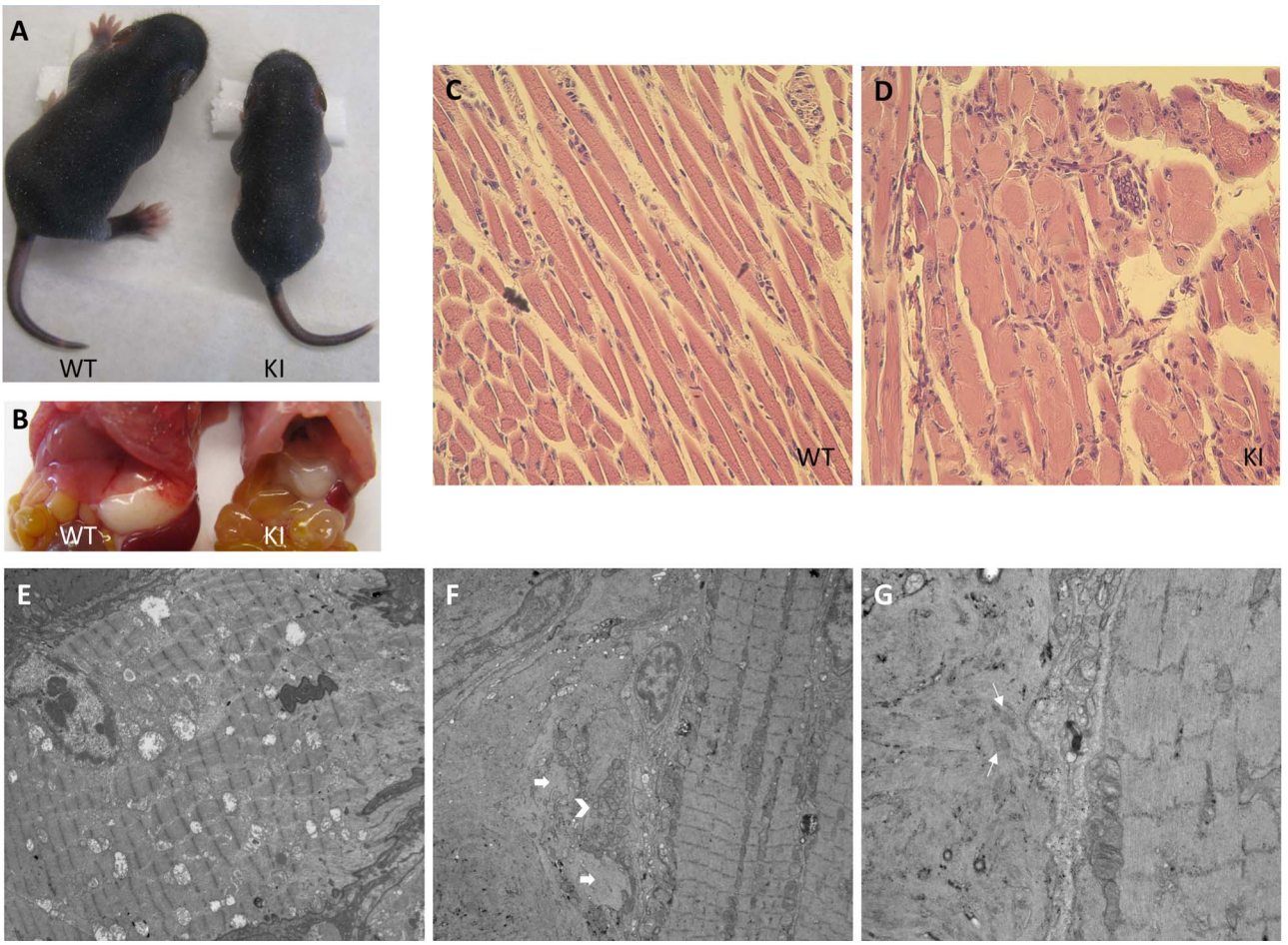

Figure 2. Phenotype of *Cfl2*$^{A35T/A35T}$ mice. (**A**) KI mice were significantly smaller than the WT littermate controls. (**B**) The stomach bubble is seen to be empty in KI mice, whereas it is distended in WT littermate controls. (**C** and **D**) H&E staining of quadriceps muscle sections from WT (C) and KI (D) mice at P7 (images taken at 40× magnification). Degenerating swollen muscle fibers with vacuoles are visible in the muscle sections of the KI mice (D). (**E–G**) Transmission EM images demonstrate ultrastructural defects in KI quadriceps sections (F and G; scale bar = 2 µm and 500 nm, respectively) relative to healthy WT controls (E; scale = 2 µm) at P7. KI muscle showed marked disorganization and sarcomeric disruption in some myofibers adjacent to healthy fibers (G). Also observed in KI muscle were actin accumulations (white arrows, G), nemaline bodies (white block arrows, F), and mitochondrial accumulations (white arrowhead, F).

Phenotyping of *Cfl2*$^{A35T/A35T}$ mice

The KI mice were indistinguishable from their WT littermates at birth and were born in expected Mendelian ratios, but began to demonstrate growth defects that were observable by post-natal day (P) 3 and statistically significant by by P7 (Fig. 2A), and none survived past P9. KI mice weighed an average of 2.7 ± 0.2 g, whereas the average WT weight was nearly twice as large at 4.8 ± 0.4 g ($P < 0.00001$), and the average length of KI mice was 41.8 ± 1.5 mm relative to a WT average length of 48.5 ± 3.5 mm ($P < 0.01$). In addition, gross observation revealed that KI mice contained minimal milk in their stomachs compared with WT littermates at P7 (Fig. 2B), indicating that their ability to suckle was reduced, likely due to muscle weakness.

We have previously used our *Cfl2*-KO mouse model to demonstrate that cofilin-2 is not critical for myofibrillogenesis but is required for early post-natal muscle maintenance (11). In order to evaluate the effect of the p.A35T mutation on this protein function, we performed histopathological analysis on quadriceps tissue from KI and WT mice at P7. Light microscopy of haematoxylin and eosin (H&E)-stained sections revealed severe ballooning degeneration of muscle fibers with vacuoles (Fig. 2C and D), indicating that early post-natal muscle maintenance was disrupted due to the mutation.

In order to evaluate the muscle structure of *Cfl2*$^{A35T/A35T}$ mice more precisely, electron microscopy (EM) was performed on quadriceps tissue from KI and WT mice. KI muscle tissue at P7 displayed disorganization and sarcomeric disruption in degenerating myofibers adjacent to healthy myofibers (Fig. 2E–G). Actin accumulations, nemaline bodies and mitochondrial accumulations were also observed in KI muscle and were absent in WT.

In addition, abnormally large alveolar spaces were noted in lungs of the KI mice at P7 upon routine histopathological examination (Supplementary Material, Fig. S1).

Altered expression of cofilins and actin in *Cfl2*$^{A35T/A35T}$ mice

In order to determine the effect of the mutation on cofilin-2 protein expression, levels of cofilin-2 were evaluated in major organs of KI mice by western blotting and compared with WT littermate controls (Fig. 3A and B). Results of these analyses revealed absent cofilin-2 protein in several organs including skeletal muscles, heart, brain, lungs and kidney of the KI mice.

In addition, an increase in the skeletal actin was noted in skeletal muscles and the heart of the KI mice, consistent with

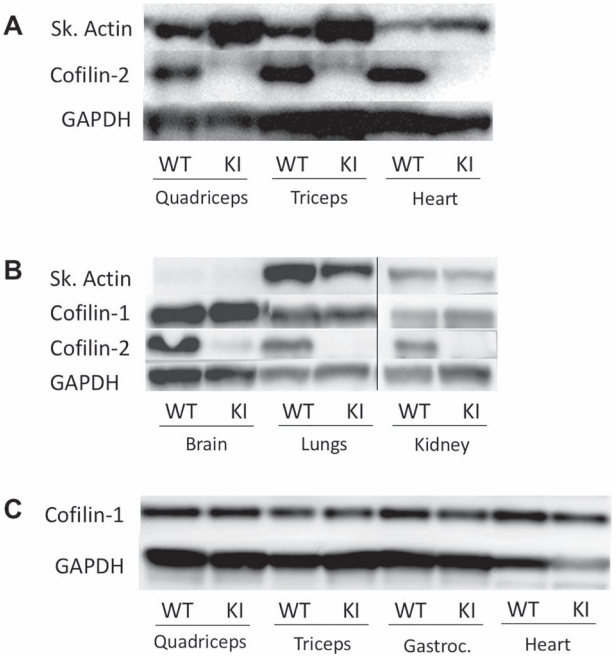

Figure 3. Western blot analysis of sarcomeric protein expression in skeletal muscle, heart, and other tissues from *Cfl2*$^{A35T/A35T}$ mice. (**A–C**) Immunoblot analysis of cofilin-2 and other sarcomeric protein levels in several tissues derived from P7 KI and WT mice in duplicate. Cofilin-2 levels were negligible in quadriceps, triceps, heart, brain, lungs and kidney of KI mice, whereas WT showed strong expression of this protein in each of these tissues (A and B). Skeletal actin levels were increased in the quadriceps, triceps, and heart of KI mice relative to WT (A and B). Cofilin-1 levels in all tested tissues were essentially unchanged in KI relative to WT (B and C). GAPDH was used as a loading control for all western blots. Thin vertical black line (B) marks where the original gel image was spliced to remove two irrelevant lanes.

lack of actin depolymerization activity due to cofilin-2 loss-of-function (Fig. 3A and B). Cofilin-1 levels were similar between WT and KI in skeletal muscles, heart, brain, lungs and kidney (Fig. 3B and C), indicating lack of compensation by cofilin-1 in response to cofilin-2 deficiency.

Alternative splicing of *CFL2* in mouse and human tissues

In order to determine the impact of the p.A35T mutation on mRNA expression, RT-PCR analysis was performed on RNA extracted from quadriceps muscles of WT, KI and heterozygous (Het) mice using primers designed to target exons 1 and 4 of *Cfl2*. Agarose gel analysis and Sanger sequencing revealed the presence of three distinct transcripts in each genotype (Fig. 4A): one corresponding to the full-length cofilin-2 transcript (FLCT) (520 bp) and two corresponding to transcripts generated by differential splicing of exon 2. The larger alternate transcript (LAT) was of 377 bp size and included the first 165 bp of exon 2, whereas the smaller alternate transcript (SAT) was of 266 bp and included only the first 54 bp (Fig. 4B). In the WT mouse, the FLCT was predominantly expressed, and the alternate transcripts LAT and SAT were expressed at very low levels. In comparison, the KI mice demonstrated significant upregulation of the SAT along with a marked reduction in FLCT. In Het mice, FLCT levels were intermediate, less than in WT but more than in KI. Further, both the alternate transcripts contained a frame shift resulting in gain of premature termination codon (PTC) postulated to encode for truncated and non-functional proteins likely targeted for degradation *in vivo*. These frameshifts were located at positions p.Val57GlyfsTer3 and p.Val20GlyfsTer3 in LAT and SAT, respectively.

We also evaluated the effect of the variant on mRNA expression in other major mouse organs including gastrocnemius, brain, kidney, liver, heart and lung. They all revealed alternative splicing of *Cfl2* in a pattern similar to that seen in quadriceps muscle (Supplementary Material, Fig. S2).

In order to evaluate the impact of the p.A35T mutation on splicing in humans, we first used the *in silico* tool, Human Splicing Finder, which predicted that the variant would result in the disruption of an exonic splice enhancer (ESE) site, potentially causing alterations in splicing. Subsequently, RT-PCR was performed on RNA samples extracted from quadriceps muscle biopsy samples of the patient (PT) and two healthy controls (CTRL1 and CTRL 2) using primers targeting exons 1 and 4 of human *CFL2*. The full-length *CFL2* transcript was represented by a band at 611 bp on agarose gel analysis, which was markedly reduced in patient relative to controls (Fig. 4C). An alternate transcript (357 bp), size consistent with SAT in mice, was also seen in both patient and controls.

Discussion

Cofilin-2 is involved in severing and depolymerization of actin filaments (13,14). We have previously linked a homozygous mutation in *CFL2* with NM/CM phenotype in two siblings within a consanguineous family (6) and created a *Cfl2*-KO mouse model that recapitulated the human disease phenotype (11). We now describe a KI mouse model of the human p.A35T mutation to further elucidate the molecular mechanisms underlying the disease caused by the mutation. The *Cfl2*$^{A35T/A35T}$ mice were very similar to the *Cfl2*-KO mice (Table 1), including significantly smaller size and weight at early postnatal stages and early lethality by P9. Further, myofiber degeneration and actin accumulations in skeletal muscle and abnormally large alveolar spaces in lung tissue were observed in KI mice, comparable to the KO mouse (11). Lack of cofilin-2 was noted in KI muscle, as was previously seen in the KO mouse (11) and human patient (6).

Our previous expression studies of the mutant p.A35T-cofilin-2 in bacteria have suggested that this mutation induces protein misfolding and insolubility, likely leading to its degradation *in vivo* (6). The current study suggests that the p.A35T variant may additionally affect normal splicing resulting in reduced levels of full length CFL2, as evidenced by KI mouse and human patient data. Further, the predominant expression of the two smaller alternate transcripts in KI mice, normally present at very low levels in WT, suggests an increase in alternative splicing that introduces premature stop codons (*LAT*: p.Val57GlyfsTer3; *SAT*: p.Val20GlyfsTer3), making them targets for nonsense-mediated decay (NMD). This splicing effect was only observed in the mice and may be unique to the murine phenotype. However, a limited quantity of patient sample was available for research, and therefore additional experiments to thoroughly explore this possible splicing effect could not be conducted.

Exon skipping as a result of missense mutations has been reported in various cases (15–20), corroborating the notion that cofilin-2 loss-of-function in patients and mice carrying the p.A35T mutation may result from a splicing defect. The *in silico* analysis of this mutation indicated disruption of an exonic splice enhancer (ESE) sequence normally present in the second exon of *Cfl2*; these sequences are *cis*-acting regulatory

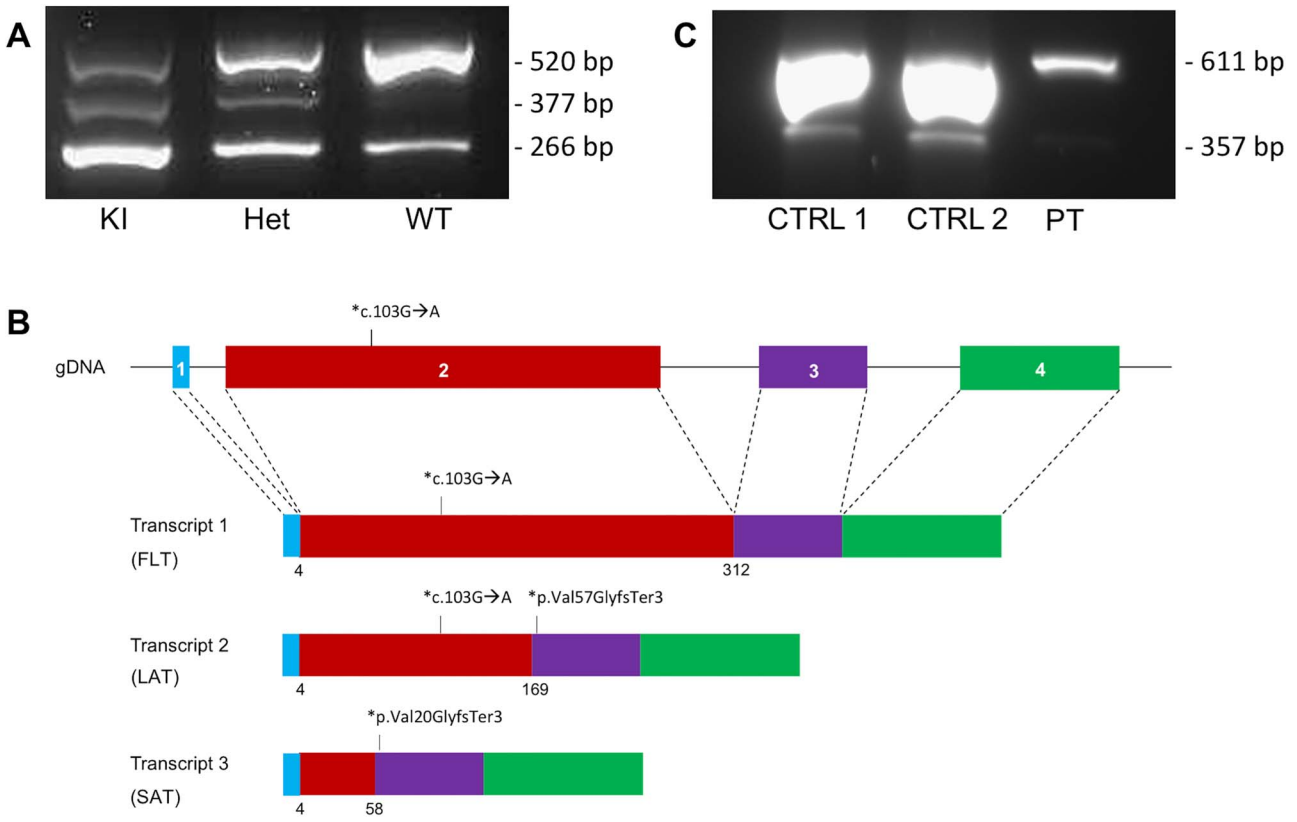

Figure 4. Exon skipping in skeletal muscle from *Cfl2*$^{A35T/A35T}$ mice. (**A**) Agarose gel analysis of the *Cfl2* RT-PCR products derived from RNA extracted from quadriceps tissue of KI and control mice using primers targeting exons 1 to 4. The band at 520 bp represents the FLCT, expressed predominantly in WT and at low levels in KI. The bands at 377 bp and 266 bp represent the LAT and SAT, respectively, expressed predominantly in KI and at very low levels in WT. Het mice display co-predominance of the full-length and alternate transcripts. (**B**) Schematic representation of alternate transcripts arising from differential splicing of *Cfl2*. The four exons of *Cfl2* and location of the mutation are identified on gDNA and transcripts. The full-length transcript contains the full second exon (308 bp); the longer alternate transcript (LAT) and shorter alternate transcript (SAT) contain only the first 165 bp and the first 54 bp of exon 2, respectively. The locations of the frame shifts arising from alternative splicing and causing premature termination are indicated on LAT and SAT. (**C**) Agarose gel analysis of *CFL2* RT-PCR products derived from RNA extracted from quadriceps tissue of the patient and two healthy controls using primers that probe for exons 1 to 4. The full-length transcript is represented by the band at 611 bp, and an alternate transcript consistent with SAT is represented by the band at 357 bp. Levels of both transcripts were markedly reduced in patient relative to both controls.

elements responsible for promoting constitutive and regulated splicing of the exon in which they reside (21). In several reports, interruptions in ESEs have been associated with aberrant splicing and exon skipping (16,17,19,20,22–25). Understanding the mechanism of exon skipping in *CFL2* has significant clinical implications, as therapeutic approaches may be developed to target the aberrant splicing.

In summary, we have created a KI mouse model of the human CFL2 variant p.A35T that essentially mimics the *Cfl2*-KO mouse previously described by us (11). Cofilin-2 deficiency in the KI mouse is likely a consequence of splicing defects resulting in shorter transcripts subject to NMD. Reduced cofilin-2 expression was also noted in the human patient's muscle, suggestive of a similar underlying mechanism. We hypothesize that the p.A35T-*CFL2* mutation in humans causes splicing defects in addition to protein misfolding which was suggested by our previous bacterial expression experiments (6). This study emphasizes the importance of evaluating the potential effects of missense variants on splicing in order to improve our understanding of the molecular mechanisms underlying disease and reveal new strategies for the development of targeted therapies.

Materials and Methods

Animal studies

All studies were performed with approval from the institutional animal care and use committee at Children's Hospital Boston (Boston, MA).

Gene targeting, generation of *Cfl2*$^{A35T/A35T}$ mice and sequencing strategy

Cfl2$^{A35T/A35T}$ mouse generation was performed by inGenious Targeting Laboratory (Ronkonkoma, NY). A ~8.9 kb region used to construct the targeting vector was first sub cloned from a positively identified C57BL/6 N BAC clone (RPCI-23) using a homologous recombination-based technique. A pGK-gb2 loxP/FRT-flanked Neo cassette was inserted downstream of exon 2. The G to A point mutation in exon 2 was generated by PCR mutagenesis. The PCR product carrying the mutation was then used to replace the wild type sequence using conventional ligation methods. The BAC was subcloned into a ~2.4 kb pSP72 (Promega) backbone vector containing an ampicillin selection cassette (Fig. 1A). The targeting construct was linearized using

Table 1. Phenotypic and Genotypic comparison of the *CFL2* mutation-associated human disease and *Cfl2-KO* and KI mouse models

	Patient (p.A35T mutation in *CFL2*)	Cfl2-KI mouse ($Cfl2^{A35T/A35T}$)	Cfl2-KO mouse ($Cfl2^{-/-}$)
Phenotype:	Hypotonia at birth - Delayed early motor milestones, frequent falls, inability to run - Diagnosed with NM at 2 years - Ambulant at 9 years	- Growth defects observed by P3, statistically significant by P7 - Early lethality (died by P9) - Empty stomach indicates inability to suckle (muscle weakness) - Reduced mobility/movement	- Growth defects observed by P3, statistically significant by P7 - Early lethality (died by P8) - Empty stomach indicates inability to suckle (muscle weakness) - Reduced mobility/movement
Histopathology:			
Skeletal muscle	- Occasional minicores and nemaline bodies	- Ballooning degeneration of muscle fibers	- Ballooning degeneration of muscle fibers
Other tissues/organs	- Not evaluated	- Abnormally large alveolar spaces in lungs	- Abnormally large alveolar spaces in lungs
Skeletal muscle ultrastructure:	- Nemaline bodies - F-actin accumulations - Minicores - Concentric laminated bodies	- Nemaline bodies - F-actin accumulations - Disorganization and sarcomeric disruption in degenerating myofibers - Mitochondrial accumulations	- Nemaline bodies - F-actin accumulations - Disorganization and sarcomeric disruption in degenerating myofibers - Mitochondrial accumulations
Protein expression:	- CFL2 protein severely reduced in muscle	- CFL2 protein absent in major organs - Skeletal actin upregulated in skeletal muscle and heart	- CFL2 protein absent in major organs - Increased levels of sarcomeric proteins (skeletal actin, alpha-actinin-2, tropomyosin) in skeletal muscle and heart
mRNA expression/splicing:	- Reduced levels of full-length transcript - Alternate transcript (357 bp) seen in quadriceps muscles from both control and patient	- Reduced levels of full-length transcript - Increased expression of two alternate transcripts (377 bp, 266 bp) with truncated exon 2 in major organs including skeletal muscle	- Lack of Cfl2 transcript

SalI prior to electroporation into ES cells. The total size of the targeting construct (including vector backbone) was ~11.3 kb.

The targeted IC1 C57BL/6 embryonic stem cells were microinjected into Balb/c blastocysts. Resulting chimeras with a high percentage black coat color were mated to wild-type C57BL/6 FLP homozygous mice to remove the Neo cassette and generate heterozygous offspring. Tail DNA was analyzed by PCR analysis for confirmation of point mutation, Neo cassette deletion and correct targeting. Primers used for amplification were forward primer PT1 (TTTAAGGCCTC-GATCGGCAGAGTTGACACAATACAGAAGG) and reverse primer F7 (GGAACTTCGCTAGACTAGTACGCGTG), which generated a 740 bp fragment. The heterozygotes were bred to obtain the homozygous mice (p.A35T+/+). Direct sequencing confirmed the presence of the mutation (Fig. 1B). The primers used to confirm the genotypes on agarose gel analysis were: 1Fa: GCTTACGTTGTTTGGTGCAG, 1R: CGGAAAAGAAAAACACACCTC and 2Fb: GCATAAGCTTGGATCCGTTC. 1Fa and 1R flanked exon 2, generating a WT band of 700 bp and a slightly larger KI band of 878 bp (due to residual Neo cassette); Het mice had both bands. There was an additional band at 281 bp in both the Het and KI from the 2Fb and 1R primers, as the 2Fb primer was present within the residual Neo cassette (Fig. 1B).

Tissue collection in mice

At 1 week of age, mice were euthanized by inhaled CO_2 and decapitated immediately prior to tissue collection in accordance with the regulations of the Institutional Animal Care and Use Committee (IACUC) at Boston Children's Hospital. Several tissues were removed during dissection including various muscle groups (quadriceps, gastrocnemius, triceps, soleus, and diaphragm) and other major organs (heart, lung, liver, kidneys, brain, and spleen). Complete autopsy was also performed on euthanized mice by the Rodent Histopathology Core at Harvard Medical School (Boston, MA).

Histological analysis

Tissue was snap-frozen in nitrogen-cooled isopentane. Frozen cross-sections (8 µm) were stained with hematoxylin and eosin (H&E) using standard protocols, and morphological analysis was conducted using an Eclipse 50i microscope (Nikon Instruments Inc., Melville, NY). Light microscopic images were captured using a SPOT Insight 4 Meg FW Color Mosaic camera and SPOT 4.5.9.1 software (Diagnostic Instruments Inc., Sterling Heights, MI).

Electron microscopy

Electron microscopy was performed as described previously (11). These methods were executed at the Electron Microscopy (EM) Core at Harvard Medical School (Boston, MA).

In silico analysis

Publicly available *in silico* tools were used to predict the effects of the c.103G>A mutation on splicing in human *CFL2*. We used

the Human Splicing Finder (HSF; available at http://www.umd.be/HSF/), an analytic tool designed to identify the effects of mutations on known splicing signals in human sequences (26).

RT-PCR analysis

RNA was extracted from mouse quadriceps tissue and patient muscle biopsy using the RNeasy Fibrous Tissue Mini Kit (Qiagen, Valencia, CA), and was then converted to cDNA using SuperScript III First-Strand Synthesis System (Invitrogen, Grand Island, NY). Specific primers designed to target murine *Cfl2* exons 1–4 (forward: GACCCCTCCTTCTTCTCGTC; reverse: GCGGTCCTTAATATCGTCCA) and human *CFL2* exons 1–4 (forward: AGTGCCACAGAGCCGAAG; reverse: GGACTGAGCTGGAGAAATGG) were used.

For real time (RT)-PCR analysis, 100 ng of cDNA was added to 10 µl of the Taqman Universal PCR Master Mix (Applied Biosystems, Carlsbad, CA) and 1 µl of the appropriate Taqman probe (Applied Biosystems) to create the RT-PCR samples. GAPDH-VIC was used as the control probe and primers for genes of interest used a FAM probe. RT-PCR was performed and analyzed using the 7300 Real Time PCR System (Applied Biosystems) and 7500 Real-Time PCR System Sequence Detection Software v1.4. The PCR program used was 50°C for 2 min, 95°C for 10 min and 40 repetitions of 95°C for 0.15 min followed by 60°C for 1 min. The relative amount of target gene expression was calculated as fold-changes relative to WT littermate controls that were normalized to GAPDH.

Western blots

Tissues from various muscles and organs were frozen at necropsy and stored at −80°C until analysis. Protein isolation and western blot procedures were performed as previously described (27). Transferred proteins were probed with antibodies against the full-length isoform of cofilin-2 (C7506–50, 1:250 dilution; US Biological, Swampscott, MA), cofilin-1 (D3F9, 1: 250 dilution, Cell Signaling, Beverly, MA), α-sarcomeric actin (5C5, 1:1000 dilution, Sigma, St.Louis, MO), and GAPDH [glyceraldehyde-3-phosphate dehydrogenase] (6C5, 1:10000 dilution; Abcam PLC, Cambridge, MA) and visualized using enhanced chemiluminescence. Adequacy of transfer was determined using Ponceau S staining. Protein levels were quantified and normalized to GAPDH expression using Quantity One software, version 4.2.1 (Bio-Rad Laboratories, Inc., Hercules, CA) on an Image Station 440 (Kodak DS; Eastman Kodak Co., Rochester, NY).

Supplementary Material

Supplementary Material is available at *HMG* online.

Acknowledgements

We wish to thank Roderick Bronson of the Rodent Histopathology Core, Harvard Medical School and Maria Ericsson, Louise Trakimas and Elizabeth Benecchi of the Electron Microscopy Core, Department of Cell Biology, Harvard Medical School.

Funding

National Institute of Health (NIH), National Institute of Arthritis and Musculoskeletal Diseases (NIAMS) (R01AR068429 to P.B.A.); the National Institute of Child Health and Human Development (NICHD) (R01HD075802); Muscular Dystrophy Association (USA) (MDA602235 to A.H.B.). Sanger sequencing was performed at the Intellectual and Developmental Disabilities Research Center (IDDRC) laboratory at Boston Children's Hospital, supported by the NICHD (U54HD090255).

Conflict of Interest: The authors have no conflicts of interest to disclose.

References

1. North, K.N., Laing, N.G. and Wallgren-Pettersson, C. (1997) Nemaline myopathy: current concepts. The ENMC International Consortium and Nemaline Myopathy. *J. Med. Genet.*, **34**, 705–713.
2. Ryan, M.M., Ilkovski, B., Strickland, C.D., Schnell, C., Sanoudou, D., Midgett, C., Houston, R., Muirhead, D., Dennett, X., Shield, L.K. *et al.* (2003) Clinical course correlates poorly with muscle pathology in nemaline myopathy. *Neurology*, **60**, 665–673.
3. Ryan, M.M., Schnell, C., Strickland, C.D., Shield, L.K., Morgan, G., Iannaccone, S.T., Laing, N.G., Beggs, A.H. and North, K.N. (2001) Nemaline myopathy: a clinical study of 143 cases. *Ann. Neurol.*, **50**, 312–320.
4. Sanoudou, D. and Beggs, A.H. (2001) Clinical and genetic heterogeneity in nemaline myopathy—a disease of skeletal muscle thin filaments. *Trends Mol. Med.*, **7**, 362–368.
5. de Winter, J.M. and Ottenheijm, C.A. (2017) Sarcomere dysfunction in Nemaline myopathy. *J. Neuromuscul. Dis.*, **4**, 99–113.
6. Agrawal, P.B., Greenleaf, R.S., Tomczak, K.K., Lehtokari, V.L., Wallgren-Pettersson, C., Wallefeld, W., Laing, N.G., Darras, B.T., Maciver, S.K., Dormitzer, P.R. *et al.* (2007) Nemaline myopathy with minicores caused by mutation of the CFL2 gene encoding the skeletal muscle actin-binding protein, cofilin-2. *Am. J. Hum. Genet.*, **80**, 162–167.
7. Fattori, F., Fiorillo, C., Rodolico, C., Tasca, G., Verardo, M., Bellacchio, E., Fagiolari, G., Lupica, A., Broda, P., Moggio, M. *et al.* (2017) Congenital myopathy with protein aggregates and nemaline bodies related to *CFL2* mutations. *Neuromuscul. Disord.*, **27**, S186.
8. Fattori, F., Fiorillo, C., Rodolico, C., Tasca, G., Verardo, M., Bellacchio, E., Pizzi, S., Ciolfi, A., Fagiolari, G., Lupica, A. *et al.* (2018) Expanding the histopathological spectrum of CFL2-related myopathies. *Clin. Genet.*, **93**, 1234–1239.
9. Ockeloen, C.W., Gilhuis, H.J., Pfundt, R., Kamsteeg, E.J., Agrawal, P.B., Beggs, A.H., Dara Hama-Amin, A., Diekstra, A., Knoers, N.V., Lammens, M. *et al.* (2012) Congenital myopathy caused by a novel missense mutation in the CFL2 gene. *Neuromuscul. Disord.*, **22**, 632–639.
10. Ong, R.W., AlSaman, A., Selcen, D., Arabshahi, A., Yau, K.S., Ravenscroft, G., Duff, R.M., Atkinson, V., Allcock, R.J. and Laing, N.G. (2014) Novel cofilin-2 (CFL2) four base pair deletion causing nemaline myopathy. *J. Neurol. Neurosurg. Psychiatry*, **85**, 1058–1060.
11. Agrawal, P.B., Joshi, M., Savic, T., Chen, Z. and Beggs, A.H. (2012) Normal myofibrillar development followed by progressive sarcomeric disruption with actin accumulations in a mouse Cfl2 knockout demonstrates requirement of cofilin-2 for muscle maintenance. *Hum. Mol. Genet.*, **21**, 2341–2356.
12. Gurniak, C.B., Chevessier, F., Jokwitz, M., Jönsson, F., Perlas, E., Richter, H., Matern, G., Boyl, P.P., Chaponnier, C., Fürst, D.

et al. (2014) Severe protein aggregate myopathy in a knockout mouse model points to an essential role of cofilin2 in sarcomeric actin exchange and muscle maintenance. *Eur. J. Cell Biol.*, **93**, 252–266.
13. Bamburg, J.R. (1999) Proteins of the ADF/cofilin family: essential regulators of actin dynamics. *Annu. Rev. Cell Dev. Biol.*, **15**, 185–230.
14. Chen, H., Bernstein, B.W., Sneider, J.M., Boyle, J.A., Minamide, L.S. and Bamburg, J.R. (2004) In vitro activity differences between proteins of the ADF/cofilin family define two distinct subgroups. *Biochemistry*, **43**, 7127–7142.
15. Liu, H.X., Cartegni, L., Zhang, M.Q. and Krainer, A.R. (2001) A mechanism for exon skipping caused by nonsense or missense mutations in BRCA1 and other genes. *Nat. Genet.*, **27**, 55–58.
16. Millevoi, S., Bernat, S., Telly, D., Fouque, F., Gladieff, L., Favre, G., Vagner, S. and Toulas, C. (2010) The c.5242C>A BRCA1 missense variant induces exon skipping by increasing splicing repressors binding. *Breast Cancer Res. Treat.*, **120**, 391–399.
17. Otsuka, H., Sasai, H., Nakama, M., Aoyama, Y., Abdelkreem, E., Ohnishi, H., Konstantopoulou, V., Sass, J.O. and Fukao, T. (2016) Exon 10 skipping in ACAT1 caused by a novel c.949G>A mutation located at an exonic splice enhancer site. *Mol. Med. Rep.*, **14**, 4906–4910.
18. Thomassen, M., Kruse, T.A., Jensen, P.K. and Gerdes, A.M. (2006) A missense mutation in exon 13 in BRCA2, c.7235G>A, results in skipping of exon 13. *Genet. Test.*, **10**, 116–120.
19. Yang, Y., Swaminathan, S., Martin, B.K. and Sharan, S.K. (2003) Aberrant splicing induced by missense mutations in BRCA1: clues from a humanized mouse model. *Hum. Mol. Genet.*, **12**, 2121–2131.
20. Zatkova, A., Messiaen, L., Vandenbroucke, I., Wieser, R., Fonatsch, C., Krainer, A.R. and Wimmer, K. (2004) Disruption of exonic splicing enhancer elements is the principal cause of exon skipping associated with seven nonsense or missense alleles of NF1. *Hum. Mutat.*, **24**, 491–501.
21. Blencowe, B.J. (2000) Exonic splicing enhancers: mechanism of action, diversity and role in human genetic diseases. *Trends Biochem. Sci.*, **25**, 106–110.
22. Cartegni, L. and Krainer, A.R. (2002) Disruption of an SF2/ASF-dependent exonic splicing enhancer in SMN2 causes spinal muscular atrophy in the absence of SMN1. *Nat. Genet.*, **30**, 377–384.
23. Fackenthal, J.D., Cartegni, L., Krainer, A.R. and Olopade, O.I. (2002) BRCA2 T2722R is a deleterious allele that causes exon skipping. *Am. J. Hum. Genet.*, **71**, 625–631.
24. Farrugia, D.J., Agarwal, M.K., Pankratz, V.S., Deffenbaugh, A.M., Pruss, D., Frye, C., Wadum, L., Johnson, K., Mentlick, J., Tavtigian, S.V. *et al*. (2008) Functional assays for classification of BRCA2 variants of uncertain significance. *Cancer Res.*, **68**, 3523–3531.
25. Pagani, F. and Baralle, F.E. (2004) Genomic variants in exons and introns: identifying the splicing spoilers. *Nat. Rev. Genet.*, **5**, 389–396.
26. Desmet, F.O., Hamroun, D., Lalande, M., Collod-Béroud, G., Claustres, M. and Béroud, C. (2009) Human splicing finder: an online bioinformatics tool to predict splicing signals. *Nucleic Acids Res.*, **37**, e67.
27. Wattanasirichaigoon, D., Swoboda, K.J., Takada, F., Tong, H.Q., Lip, V., Iannaccone, S.T., Wallgren-Pettersson, C., Laing, N.G. and Beggs, A.H. (2002) Mutations of the slow muscle alpha-tropomyosin gene, TPM3, are a rare cause of nemaline myopathy. *Neurology*, **59**, 613–617.